Crystal Structure of the S-Nitroso Form of Liganded Human Hemoglobin[†,‡]

Nei-Li Chan, Paul H. Rogers, and Arthur Arnone*

Department of Biochemistry, College of Medicine, The University of Iowa, Iowa City, Iowa 52242

Received July 14, 1998; Revised Manuscript Received September 21, 1998

ABSTRACT: Although numerous reports have documented that the S-nitrosylation of cysteine residues by NO alters the activities of a wide variety of proteins, the direct visualization and the structural consequences of this reversible modification have not yet been reported for any protein. Here we describe the crystal structure of *S*-nitroso-nitrosylhemoglobin determined at a resolution of 1.8 Å. The specific reaction of NO with Cys93β is confirmed in this structure, and a large S-nitrosylation-induced change in the tertiary structure of the COOH-terminal dipeptides of the β subunits provides additional insight into the stereochemical mechanism by which blood flow is regulated by the interaction of NO with hemoglobin.

In addition to its well-studied direct role in efficient oxygen transport, recent studies strongly suggest that human hemoglobin A (HbA) also actively participates in the regulation of blood flow by transporting the vasorelaxant nitric oxide (NO) to hypoxic tissues and by scavenging NO in tissues where oxygen is plentiful. Specifically, Stamler and coworkers (*1*, *2*) have shown that HbA undergoes S-nitrosylation (SNO-HbA) in vitro and in vivo, that the site of S-nitrosylation is likely the reactive thiol group of Cys93β, and that the rate and extent of S-nitroso formation is much greater for oxygenated hemoglobin (oxyHbA) than for deoxyhemoglobin (deoxyHbA).

The studies from the Stamler lab suggest the following mechanism for the regulation of blood flow by SNO-HbA. In the lungs, where the partial O_2 pressure (PO_2) is high, HbA exists predominantly as oxyHbA which rapidly binds NO and forms SNO-oxyHbA. In vivo, SNO-oxyHbA is thought to form via a transnitrosation reaction with *S*-nitrosoglutathione (GSNO) (*1*, *2*) as well as by intrasubunit NO group exchange between a nitrosylated β heme group and Cys93β (*3*). After leaving the lungs, circulating SNO-oxyHbA is exposed to a range of PO_2 levels that reflect the local metabolic state. In tissues with low PO_2, where O_2 requirements are high, SNO-oxyHbA releases bound O_2. Deoxygenation of HbA reduces its affinity for NO and leads to the release of NO, either as free NO or as GSNO. The reactive NO may be immediately rebound to a vacant heme site (*3*), whereas the more stable GSNO may promote the influx of O_2 into hypoxic tissues by diffusing into nearby smooth muscle tissue, dilating blood vessels, and thereby increasing blood flow (*1*−*3*). Conversely, in resting tissues, where both the PO_2 and the oxygen saturation of HbA are high, oxyHbA will scavenge endogenous NO generated by the endothelium and inhibit vasodilation.

To better understand the molecular basis for the linkage between S-nitrosylation and the ligand-induced allosteric transitions of HbA, we have determined the structure of crystalline SNO-nitrosylHbA (i.e., HbA in which cysteine residues have been converted to *S*-nitrosocysteine and NO is the heme ligand) prepared by directly exposing crystals of carbonmonoxyHbA to gaseous NO under anaerobic condition.

EXPERIMENTAL PROCEDURES

Preparation of Crystalline SNO-NitrosylHbA. Liganded HbA is known to exist in at least two different quaternary structures, the R-structure (*4*) and the R2-structure (*5*). In the present study, crystalline SNO-nitrosylHbA was prepared by direct exposure of an R2 crystal form of carbonmonoxyHbA to gaseous NO under anaerobic condition. Specifically, a single crystal of carbonmonoxyHbA was placed in a 2 cm^3 vial and soaked overnight in 0.5 mL of a deoxygenated substitute mother liquor containing 16.4% poly(ethylene glycol) 6000 and 100 mM sodium cacodylate at pH 5.8. Next, the vial was flushed with 3 cm^3 of gaseous NO and stoppered, and the crystal was soaked for another day under these conditions before it was mounted in a quartz capillary tube. Before the capillary tube was sealed, it was flushed with an additional 3 cm^3 of gaseous NO. As shown in the Results and Discussion, under these experimental conditions, Cys93β1 and Cys93β2 are converted to *S*-nitrosocysteine, and the CO ligands of both the α and the β hemes are replaced by NO.

Data Collection. Diffraction data were collected with a Rigaku AFC6 four-circle diffractometer fitted with a San Diego Multiwire Systems area detector. Each data set was scaled and merged according to the procedure of Howard et al. (*6*). To determine if the reaction between NO and

[†] This work was supported by National Institutes of Health Program Project Grant PO1 HL51084. N.-L.C. was also supported by a fellowship from the Iowa Affiliate of the American Heart Association.

[‡] Refined coordinates and structure factors have been deposited in the Brookhaven Protein Data Bank. The accession numbers for the coordinates and the structure factors are 1buw and r1buwsf, respectively.

* Author to whom correspondence should be addressed. E-mail: arthur-arnone@uiowa.edu.

[1] Abbreviations: NO, nitric oxide; HbA, hemoglobin A; SNO-HbA, S-nitroso hemoglobin A; oxyHbA, oxygenated hemoglobin A; deoxyHbA, deoxyhemoglobin A; PO_2, partial O_2 pressure; GSNO, *S*-nitrosoglutathione; SNO-nitrosylHbA, *S*-nitroso nitrosylhemoglobin A; nitrosylLb, nitrosylleghemoglobin; nitrosylMb, nitrosylmyoglobin; hGR, human glutathione reductase; $GS_2Fe(NO)_2$, diglutathionyl-dinitrosoiron.

10.1021/bi9816711 CCC: $15.00
Published on Web 11/04/1998

crystalline carbonmonoxyHbA had reached equilibrium, diffraction data were collected on three crystals after they had been exposed to NO for various periods of time. Data collection on the first crystal began 3 days after exposure to NO, whereas data collection was delayed for 10 days on the second crystal and for 1 month on the last crystal. Analysis of difference electron density maps (not shown) calculated using pairwise combinations of these data sets indicates that complete S-nitrosylation of Cys93β1 and Cys93β2, as well as complete replacement of CO by NO at the α and β heme groups, was achieved before 10 days of exposure to NO. The "10 day" data set was used to determine the structure of SNO-nitrosylHbA. It is 93% complete to 1.76 Å resolution and contains 55 671 unique reflections (a total of 273 695 observations were collected, and the standard R_{merge} value is 7.0%).

Structure Determination. A difference electron density map calculated with ($F_{SNO-nitrosylHbA} - F_{carbonmonoxyHbA}$) amplitudes and phases derived from the refined R2 structure of carbonmonoxyHbA (*5*) contained three significant features: positive difference density extending from the ends of the Cys93β1 and Cys93β2 side chains, negative difference density at the positions of the β1 and β2 COOH-terminal dipeptides, and positive/negative pairs of difference density peaks flanking the position of the CO ligand on each of the heme groups. On the basis of these observations, a starting model for SNO-nitrosylHbA was constructed from the refined crystal structure of carbonmonoxyHbA by (1) converting Cys93β1 and Cys93β2 into alanine residues, (2) deleting the last five residues of each β-subunit, and (3) deleting the four CO ligands. Initial refinement of this model consisted of rigid body refinement with X-PLOR (*7*) followed by stereochemical restrained least-squares refinement with PROLSQ (*8*). Next, ($2F_{obs} - F_{calc}$) and ($F_{obs} - F_{calc}$) electron density maps were used with the TOM/FRODO software (*9*) to position S-nitroso side chains at residues 93β1 and 93β2, add residues Ala142, His143, and Lys144 to the β1 and β2 COOH-termini, and fit NO ligands to all four heme groups. Residues Tyr145β and His146β were not added to the atomic model because of the complete absence of significant electron density beyond residue Lys144β. Final refinement of the atomic model was carried out with PROLSQ. The R and R_{free} values are 18.4 and 24.4%, respectively. Stereochemical restraints for the S-nitroso groups were taken from the X-ray structure of *S*-nitroso-*N*-acetyl-penicillamine (*10*). Refinement statistics for the 1.8 Å structure of SNO-nitrosylHbA are reported in Table 1.

Table 1: Summary of PROLSQ SNO-NitrosylHbA Refinement Parameters

parameter[a]	target σ[b]	rms Δ[c]
bonding distances (Å)		
bond lengths (1−2 neighbors)	0.010	0.009
1−3 neighbors distances	0.015	0.023
1−4 planar neighbor distances	0.030	0.037
metal coordination	0.100	0.112
planar groups, deviations from plane (Å)	0.010	0.010
chiral centers, chiral volumes (Å^3)	0.080	0.119
nonbonded contacts (Å)		
separated by one torsion angle	0.200	0.158
all other van der Waals contacts	0.200	0.166
possible hydrogen bonds	0.200	0.159
conformational torsion angles (deg)		
planar (e.g., peptide ω)	5.0	2.4
staggered (e.g., aliphatic χ)	15.0	19.4
transverse (e.g., aromatic χ^2)	25.0	31.1
isotropic temperature factors (Å^2)		
main chain (1−2 neighbors)	2.0	2.0
main chain (1−3 neighbors)	3.0	2.8
side chain (1−2 neighbors)	4.0	5.0

[a] 1−2 neighbors, covalently bonded atom pairs. 1−3 neighbors, atom pairs separated by 2 covalent bonds. 1−4 planar neighbors, atom pairs in a planar group separated by three covalent bonds. [b] Target σ, estimated standard deviations, where $1/\sigma^2$ is used as a relative weighting factor in the minimized sum of observed functions. [c] rms Δ, root-mean-square deviations from ideal values (as determined from accurate small molecule crystal structures in the case of bonding distances, chiral volumes, and nonbonded contacts) or from nearest-neighbor values (in the case of isotropic temperature factors).

RESULTS AND DISCUSSION

Direct Observation of S-Nitrosocysteine. Crystalline SNO-nitrosylHbA was prepared by direct exposure of the R2 crystal form of human carbonmonoxyHbA to NO. Electron density images of the regions surrounding Cys93β1 and Cys93β2 (Figure 1, panels a and b) show that exposing a crystal of carbonmonoxyHbA to ~1 atm of gaseous NO results in the complete S-nitrosylation of both cysteine residues, confirming the solution studies of Jia et al. (*1*). Moreover, careful examination of the entire electron density map reveals that Cys93β1 and Cys93β2 are the only residues to react with NO. In particular, the four other cysteine residues of HbA (Cys104α1, Cys104α2, Cys112β1, and Cys112β2) do not react with NO, even though a very high concentration of NO was used in these experiments. This observation is consistent with the environment of the side chains of Cys104α and Cys112β (they are completely buried and are part of the tightly packed α1β1 interface) and with previous studies that showed they are much less reactive than Cys93β to a wide variety of sulfhydryl reagents in both deoxy and liganded HbA (*11*−*14*).

It has been shown previously that the S-nitrosylation reaction under anaerobic condition requires an electron acceptor, such as NAD^+ (*15*). However, *S*-nitrosocysteine was observed in this study despite the absence of an obvious electron acceptor. Recently, Gow and Stamler (*3*) found that NO can induce the formation of oxidized HbA (metHbA) under anaerobic condition. Therefore, it is possible that the transiently formed metHbA can serve as an electron acceptor and promote the S-nitrosylation reaction. Alternatively, the presence of contaminants such as O_2, other nitrogen oxides, and metal ions may also serve as electron acceptors.

S-Nitrosylation-Induced Changes in β Subunit Tertiary Structure. The reaction of NO with Cys93β produces a large change in the tertiary structure of the COOH-terminal dipeptide of both β subunits. Specifically, the addition of NO to Cys93β results in the complete disappearance of the electron density associated with Tyr145β−His146β, indicating that this dipeptide is displaced by the formation of SNO-Cys93β (see Figure 1, panels a and b). The reason for the displacement of the Tyr145β−His146β dipeptide is clear from a superposition of the β subunits of carbonmonoxyHbA and SNO-nitrosylHbA (Figure 1c); the SNO group on the side chain of residue 93β collides with the side chain of Tyr145β, ejecting the phenol group from its binding pocket between Cys93β, Pro100β, and the backbone carbonyl of Val98β.

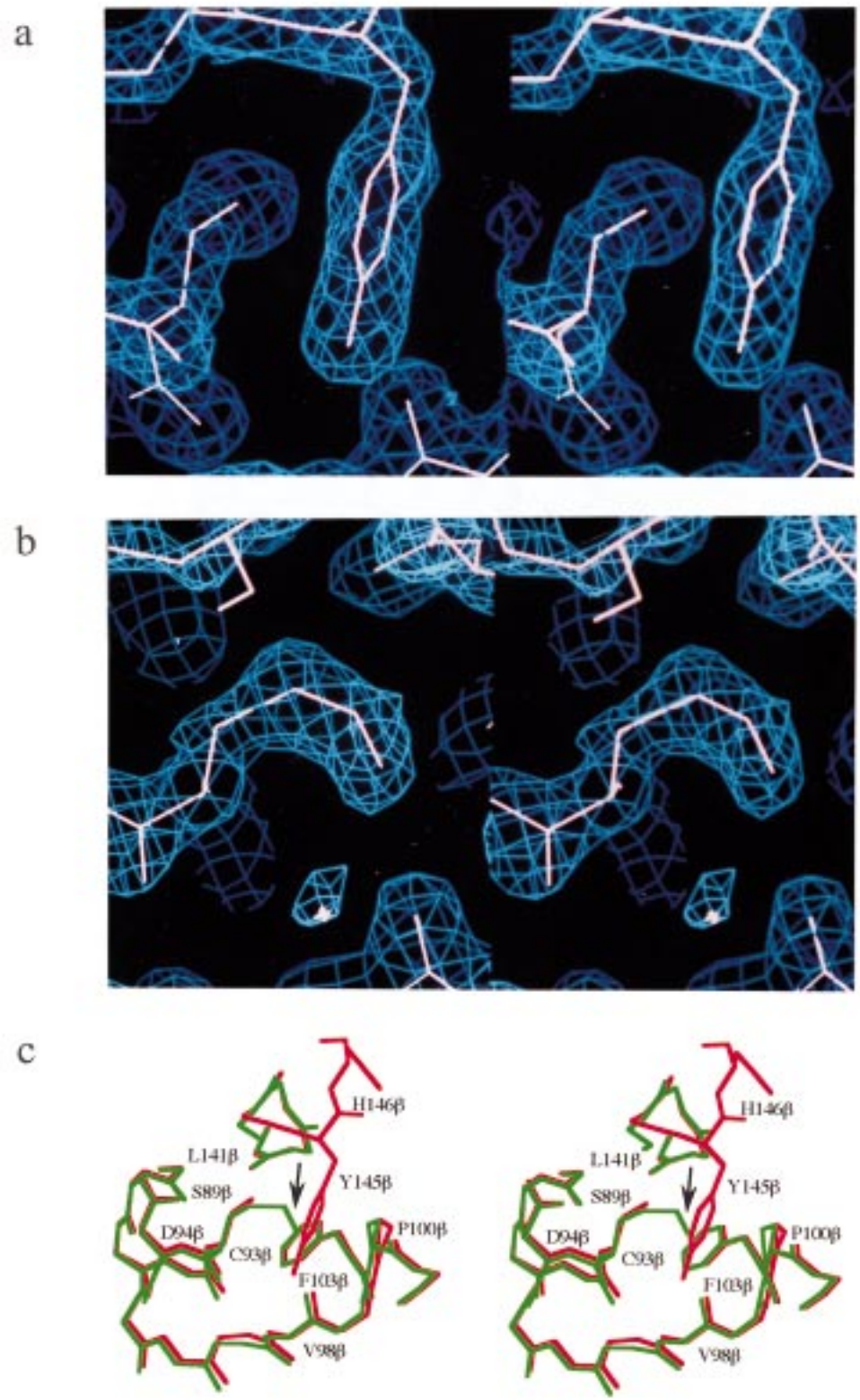

FIGURE 1: Stereodiagrams of ($2F_{obs} - F_{cal}$) electron density maps showing the environment of Cys93β1 for carbonmonoxyHbA (a) and for SNO-nitrosylHbA (b). (The corresponding electron density around Cys93β2 in the carbonmonoxyHbA and SNO-nitrosylHbA structures is of similar quality.) The environment of Cys93β1 (with side chains and labels for selected residues) is shown in panel c where the refined atomic models of carbonmonoxyHbA (red) and SNO-nitrosylHbA (green) have been superimposed. The arrow in panel c points to the S-nitroso group. In all three stereo diagrams, the region around Cys93β1 is viewed from the same direction, i.e., from the surface toward the interior of hemoglobin tetramer. Note that no electron density is observed for the COOH-terminal dipeptide, Tyr145β−His146β, in the SNO-nitrosylHbA electron density map. Residues 93 and 144−146 β1 and β2 were not included in the atomic model used to calculate the F_{calc} structure factor magnitudes and phases. The electron density contours are drawn at 1.5 times the rms density of the map.

In the liganded R2 quaternary structure of HbA (*5*), the imidazole groups of His146β1 and His146β2 are stacked against one another across the β1β2 interface. The fact that no electron density is observed for Tyr145β and His146β in

the SNO-nitrosylHbA electron density map indicates that the displaced COOH-terminal dipeptides are fully solvated and completely disordered in SNO-nitrosylHbA. Although the displacement of the β subunits COOH-termini does not lead to a large change in the quaternary structure of the $\alpha_2\beta_2$ tetramer in the crystals used in this study (compared to the R2 structure of carbonmonoxyHbA, there is only a 0.8° rotation of the $\alpha 1\beta 1$ dimer relative to the $\alpha 2\beta 2$ dimer in SNO-nitrosylHbA), the possibility remains that in solution the nitrosylation-induced rearrangement of the β subunits COOH-terminal dipeptides may result in a much larger change in the quaternary structure of liganded HbA (e.g., a shift in the equilibrium between the R and R2 structures).

Because crystals of SNO-deoxyHbA and S-nitrosylated liganded HbA in the R quaternary structure have not been produced as yet, the impact of the S-nitrosylation of Cys93β on these structures only could be inferred from hypothetical models. When the side-chain conformational angles observed for SNO-Cys93β in the R2 structure of SNO-nitrosylHbA (i.e., $\chi_1 = -55°$, $\chi_2 = -99°$, $\chi_3 = +87°$) were used to construct a model of SNO-deoxyHbA from the known high-resolution structure of deoxyHbA (*16*, *17*), the nitroso group collided with the Tyr145β. Alternatively, when the γS of Cys93β was held fixed to its original position in deoxyHbA (i.e., $\chi_1 = +175°$) with χ_2 and χ_3 set to the values observed in the SNO-nitrosylHbA structure, steric conflicts developed with the side chain of Asp94β. Last, all three conformational angles were allowed to vary, and this analysis revealed that only when a high energy rotamer is adopted by SNO-Cys93β ($\chi_2 \approx 0°$) can steric repulsion with surrounding residues be minimized in the SNO-deoxyHbA tetramer. We conclude, therefore, that disordering of the β subunits COOH-termini also may occur in SNO-deoxyHbA. A similar analysis of the impact of the S-nitrosylation of Cys93β on the structure of the β subunits COOH-termini in the liganded R quaternary structure of HbA resulted in the same prediction. This prediction is supported by the X-ray diffraction studies of Moffat (*18*, *19*) on a variety of chemically modified forms of horse metHb and horse carbonmonoxyHb. In particular, he found that the modification of Cys93β in the R quaternary structure with bis(*N*-maleimidomethyl)ether, *N*-(α-bromoacetoxymethyl)maleimide, *N*-(acetoxymethyl)maleimide, *N*-phenylmaleimide, and *N*-(l-oxyl-2,2,6,6-tetramethyl-4-piperidinyl)iodoacetamide resulted in the complete displacement of Tyr145β and His146β.

Structural Basis for Ligation-Associated Differences in the Reactivity of Cys93β. Just as NO reacts more readily with Cys93β in oxyHbA than in deoxyHbA (*1*, *2*), it has long been recognized that the reactivity of Cys93β toward most other sulfhydryl reagents is much greater in liganded HbA than in deoxyHbA (*11*−*14*). One explanation for this observation could be that Cys93β is more accessible in liganded HbA than it is in deoxyHbA. However, calculations of the accessible surface area of the γS atom of Cys93β in the oxyHbA R structure (*4*), the carbonmonoxyHbA R2 structure (*5*), and the deoxyHbA structure (*16*, *17*) show that the γS atom is completely buried in both of the liganded structures of HbA, and that it is only slightly exposed (with 4 Å^2 of accessible surface area) in deoxyHbA. Therefore, differences in the accessible surface area of Cys93β in the time-averaged crystal structures of liganded and deoxyHbA cannot account for differences in the reactivity of Cys93β.

A more likely explanation for the differences in the reactivity of Cys93β is that the COOH-termini of the β subunits undergo "local unfolding" or "breathing" movements that transiently expose Cys93β to a greater extent in liganded HbA than in deoxyHbA. This possibility is strongly supported by the elegant hydrogen exchange experiments of Englander et al. (*20*) which indicate that local unfolding at the β subunits COOH-termini is increased ∼200-fold by the binding of oxygen. Similarly, high-resolution crystal structures of HbA (*4*, *5*, *16*, *17*) reveal that the mobility of the β subunits COOH-termini (as measured by refined atomic temperature factors) is much higher in liganded HbA than in deoxyHbA. Taken together, the hydrogen exchange results and the temperature factor data imply that the noncovalent interactions between the β subunits COOH-termini and adjacent regions of the HbA tetramer are weaker in liganded HbA. Therefore, the energy required to displace the COOH-termini of the β subunits should be reduced in liganded HbA.

Stereochemistry of Heme-Bound NO. Since the affinity of HbA for NO is more than 1000 times greater than it is for CO (*21*), it was anticipated that exposure of carbonmonoxyHbA crystals to gaseous NO would result in the substitution of NO for CO on both the α and the β hemes. Such a replacement was indicated in the initial ($F_{\text{SNO-nitrosylHbA}} - F_{\text{carbonmonoxyHbA}}$) difference electron density map because it contains positive/negative pairs of difference peaks flanking the position of the CO ligand on each of the heme groups. As described below, the heme-ligand stereochemistry of the refined SNO-nitrosylHbA structure confirms this expectation.

To eliminate bias prior in positioning the heme ligands in ($F_{\text{obs}} - F_{\text{calc}}$) electron density images (see Figure 2), all four heme ligands were deleted from the atomic model at the start of the refinement process for SNO-nitrosylHbA, and the previously refined R2 structure of carbonmonoxyHbA was subjected to 25 additional cycles of restrained least-squares refinement after removal of the CO ligands. In Figure 2a, the region of the α1 heme in carbonmonoxyHbA is shown along with the ($F_{\text{obs}} - F_{\text{calc}}$) electron density of the CO ligand, and consistent with other crystallographic studies (Table 2) of CO liganded hemoproteins (*22*, *23*), the CO ligand adopts a conformation that is only slightly bent. The averaged Fe−C−O bond angle is 167° for α subunits and 164° for β subunits in the refined model of carbonmonoxyHbA. In contrast, crystallographic studies of nitrosometalloporphyrins have reported Fe−N−O bond angles of ∼140° (*24*, *25*). This type of bent ligand geometry clearly is evident in the SNO-nitrosylHbA ligand electron density shown in Figure 2b, and the averaged Fe−N−O bond angle is 131° for α subunits and 123° for β subunits in the final refined model of SNO-nitrosylHbA, confirming that the CO ligands have been replaced by NO. Another predicted consequence of the replacement of CO by NO is the lengthening of the bond between the heme Fe and the $N^{\epsilon 2}$ atom of the proximal histidine (Fe−$N^{\epsilon 2}$His87α/Fe−$N^{\epsilon 2}$-His92β) (*23*, *26*). In SNO-nitrosylHbA, the averaged Fe−$N^{\epsilon 2}$His bond length is 2.28 Å, in contrast to the 2.12 Å value in the refined structure of carbonmonoxyHbA.

In addition to the SNO-nitrosylHbA structure, two other high-resolution nitrosylheme protein structures recently have been reported: the 1.8 Å structure of nitrosylleghemoglobin (*23*) (nitrosylLb), and the 1.7 Å structure of nitrosylmyo-

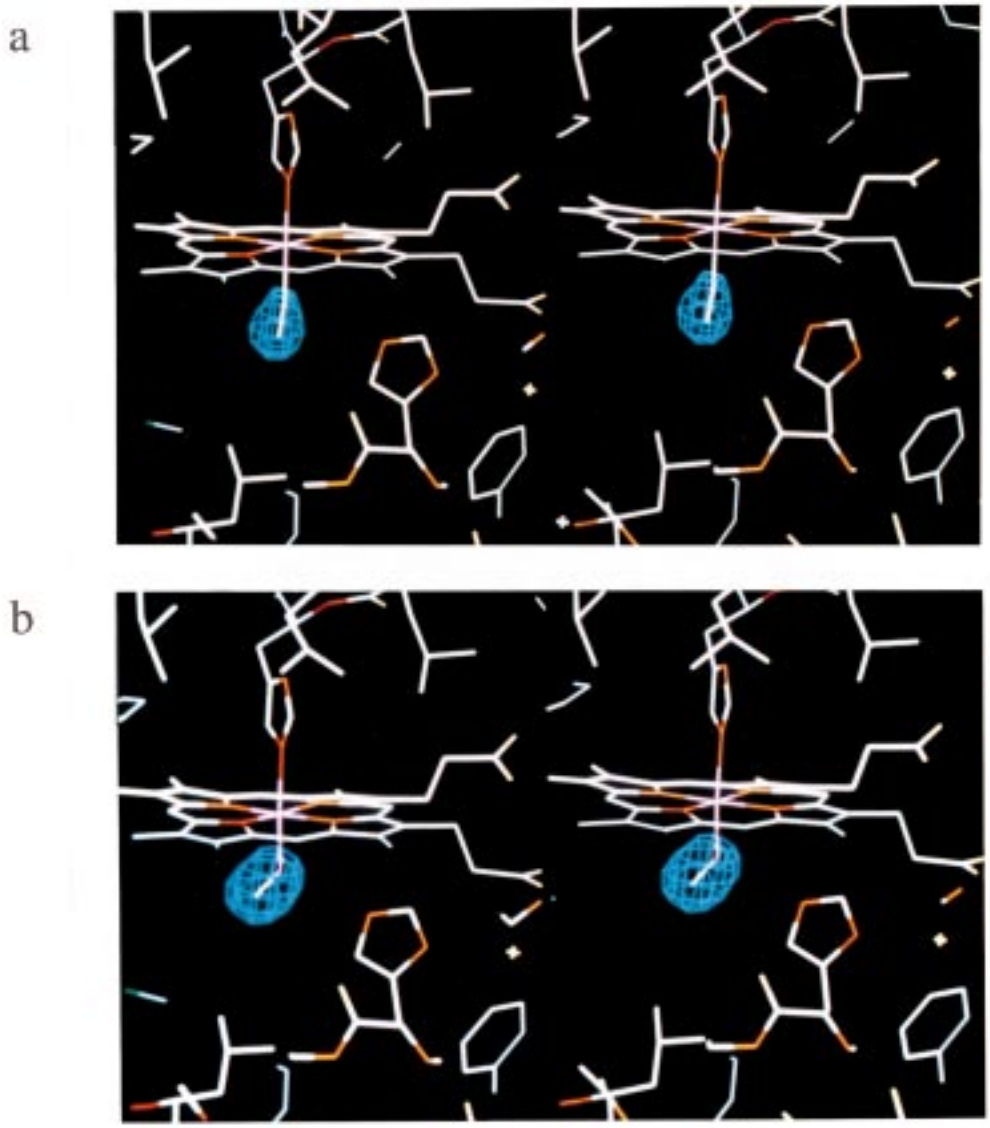

FIGURE 2: Stereoviews of ($F_{obs} - F_{calc}$) difference electron density maps showing ligand binding to the α1 heme group in carbonmonoxyHbA (a) and SNO-nitrosylHbA (b). (The corresponding electron density at the α2, β1, and β2 heme groups in the carbonmonoxyHbA and SNO-nitrosylHbA structures is of the same quality.) The CO and NO ligands were omitted from the atomic models during PROLSQ least-squares refinement, and they were not included in the atomic models used to calculate the F_{calc} structure factor magnitudes and phases. The electron density contours are drawn at 6 times the rms density of the map.

Table 2: Heme−Ligand Stereochemistry in Various Heme−NO/CO Structures

structure	Fe−HisN$^{\epsilon 2}$ (Å)	Fe−N/Fe −C (Å)	N−O/C−O (Å)	Fe−N−O/Fe−C−O (deg)	ref
Fe^{II}(NO)TPP(1-MeIm)[a]	2.18	1.74	1.14, 1.12[b]	138, 142[b]	*24*
Fe^{II}(CO)PPP(1,2-Me$_2$Im)[a]	2.08	1.77	1.15	173	*30*
carbonmonoxyHbA[c]	2.12, 2.12	1.78, 1.77	1.18, 1.18	167, 164	this paper
SNO-nitrosylHbA[c]	2.28, 2.28	1.75, 1.74	1.13, 1.11	131, 123	this paper
nitrosylLb	2.22	1.72	1.22	147	*23*
nitrosylMb	2.18	1.89	1.15	112	*26*

[a] TPP, tetraphenylporphyrin; 1-MeIm, 1-methylimidazole; PPP, 5,10,15-[(1,3,5-benzenetriyltriacetyl) tris(α,α,α-o-aminophenyl)]-20-(α-o-pivalamidophenyl)porphyrin; 1,2-Me$_2$Im, 1,2-dimethylimidazole. [b] Nitric oxide oxygen is disordered. [c] The first and second values for each parameter are, respectively, the averaged values for the α subunits and the β subunits. The Fe−HisN$^{\epsilon}$2 and Fe−N(C) bond lengths were refined by adjusting the corresponding PROLSQ target distance until it matched the refined bond length (see ref *30*). The Fe−N−O/Fe−C−O bond angles were not restrained. Each value is the average over all four subunits.

globin (*26*) (nitrosylMb). As shown in Table 2, the averaged Fe−N−O bond angle in SNO-nitrosylHbA is 127°, a value that lies between the 147° Fe−N−O bond angle nitrosylLb and the 112° Fe−N−O bond angle in nitrosylMb. This implies that increased levels of π-bonding exist between the heme Fe and the NO ligand in SNO-nitrosylHbA and nitrosylLb, an inference that is consistent with the significantly longer Fe−NO bond length in the nitrosylMb structure (1.89 Å in nitrosylMb versus 1.74−1.72 Å in the SNO-nitrosylHbA and nitrosylLb). It has been suggested by Brucker et al. (*26*) that the major environmental influence on the Fe−N−O bond angle may be an electrostatic

interaction with the distal histidine. In particular, they noted that a shorter distance between the nitrogen atom of the NO ligand and the $N^{\epsilon 2}$ atom of the distal histidine (i.e., a stronger $N\cdots HN^{\epsilon 2}$ hydrogen bond) correlates with a smaller Fe−N−O bond angle. This conjecture is supported by the averaged value of this distance that we observe in SNO-nitrosylHbA, 3.13 Å; it is longer than that reported for nitrosylMb (2.8 Å) and shorter than that reported for nitrosylLb (3.3 Å).

General Implications. In vivo, the reactive thiol groups of cysteine residues can be modified by a wide range of reactions with O_2, low molecular weight thiols, NO, and various NO-donating molecules (*27*). Recently, Becker et al. (*28*) reported crystal structures of human glutathione reductase (hGR) inactivated by GSNO and by diglutathionyl-dinitroso-iron [$GS_2Fe(NO)_2$]. Under the conditions of their study (that included exposure to atmospheric oxygen for the time period required to grow the crystals and collect the diffraction data), it was found that the active-site residue Cys63 of hGR is oxidized to form cysteine sulfenic acid (−SOH) after modification with GSNO and cysteine sulfinic acid ($-SO_2H$) after modification with $GS_2Fe(NO)_2$. Moreover, the S-nitrosylation of cysteine was not detected under their experimental conditions, supporting the concept that oxidative reactions may be a mechanism for the NO-based inactivation of enzymes. In commenting on this work, Stamler and Hausladen (*27*) argue that, in general, reversible posttranscriptional modifications, such as S-nitrosothiols and cysteine sulfenic acid, are used for signaling/regulatory functions, whereas irreversible modifications, such as cysteine sulfinic acid, typically reflect the result of long periods of nitrosative and oxidative stress. They also point out that since *S*-nitrosocysteine is among the most unstable forms of modified cysteine, it may be difficult to detect in a standard crystallographic experiment where "crystallization and data accumulation take place on time scales that are much longer than the lifetime of most S-nitrosothiols, and air, X-rays, contaminant metals and other minor reactants found in solutions of GSNO and $GS_2Fe(NO)_2$ can dramatically influence the redox-related product". By working with pure NO under anaerobic conditions, we have avoided potential problems associated with O_2 related oxidation of the S-nitroso form of HbA. However, as pointed out by DeMaster et al. (*29*), free sulfhydryl groups can be oxidized by NO itself to sulfenic acid under anaerobic conditions. Therefore, the fact that sulfenic acid is not observed in this study implies that *S*-nitrosocysteine is the most stable reaction product in the fully liganded R2 structure of HbA. In vivo, SNO-oxyHbA may form via a transnitrosation reaction with GSNO, but the structural consequences of the S-nitrosylation should be very similar to those observed in the crystal structure of SNO-nitrosylHbA.

REFERENCES

1. Jia, L., Bonaventura, C., Bonaventura, J., and Stamler, J. S. (1996) *Nature 380*, 221−226.
2. Stamler, J. S., Jia, L., Eu, J. P., McMahon, T. J., Demchenko, I. T., Bonaventura, J., Gernert, K., and Piantadosi, C. A. (1997) *Science 276*, 2034−2037.
3. Gow, A. J., and Stamler, J. S. (1998) *Nature 391*, 169−173.
4. Shaanan, B. (1983) *J. Mol. Biol. 171*, 31−59.
5. Silva, M. M., Rogers, P. H., and Arnone, A. (1992) *J. Biol. Chem. 267*, 17248−17256.
6. Howard, A. J., Nielson, C., and Xuong, N. H. (1985) *Methods. Enzymol. 114*, 452−472.
7. Brünger, A. T. (1992) X-PLOR, version 3.1, Yale University Press, New Haven and London.
8. Hendrickson, W. A. (1985) *Methods Enzymol. 115*, 252−270.
9. Jones, T. A. (1985) *Methods Enzymol. 115*, 157−189.
10. Carnahan, G. E., Lenhert, P. G., and Ravichandran, R. (1978) *Acta Crystallogr., Sect. B 34*, 2645−2648.
11. Riggs, A. (1961) *J. Biol. Chem. 236*, 1948−1954.
12. Benesch, R. E., and Benesch, R. (1962) *Biochemistry 1*, 735−738.
13. Geraci, G., and Parkhurst, L. J. (1973) *Biochemistry 12*, 3414−3418.
14. Chiancone, E., Currell, D. L., Vecchinni, P., Antonini, E., and Wyman, J. (1970) *J. Biol. Chem. 245*, 4105−4511.
15. Gow, A. J., Buerk, D. G., and Ischiropoulos, H. (1997) *J. Biol. Chem. 272*, 2841−2845.
16. Fermi, G., Perutz, M. F., Shaanan, B., and Fourme, R. (1984) *J. Mol. Biol. 175*, 159−174.
17. Kavanaugh, J. S., Rogers, P. H., Case, D. A., and Arnone, A. (1992) *Biochemistry 31*, 4111−4121.
18. Moffat, J. K. (1971) *J. Mol. Biol. 55*, 135−146.
19. Moffat, J. K. (1971) *J. Mol. Biol. 58*, 79−88.
20. Englander, S. W., Englander, J. J., McKinnie, R. E., Ackers, G. K., Turner, G. J., Westrick, J. A., and Gill, S. J. (1992) *Science 256*, 1684−1687.
21. Olson, J. S., Rohlfs, R. J., and Gibson, Q. H. (1987) *J. Biol. Chem. 262*, 12930−12938.
22. Quillin, M. L., Arduini, R. N., Olson, J. S., and Phillips, G. N., Jr. (1993) *J. Mol. Biol. 234*, 140−155.
23. Harutyunyan, E. H., Safonova, T. N., Kuranova, I. P., Popov, A. N., Teplyakov, A. V., Obmolova, G. V., Vainshtein, B. K., Dodson, G. G., and Wilson, J. C. (1996) *J. Mol. Biol. 264*, 152−161.
24. Scheidt, W. R., and Piciulo, P. L. (1976) *J. Am. Chem. Soc. 98*, 1913−1919.
25. Scheidt, W. R. (1980) *Acc. Chem. Res. 10*, 339−345.
26. Brucker, E. A., Olson, J. S., Ikeda-Saito, M., and Phillips, G. N., Jr. (1998) *Proteins 30*, 352−356.
27. Stamler, J. S., and Hausladen, A. (1998) *Nat. Struct. Biol. 5*, 247−249.
28. Becker, K., Savvides, S. N., Keese, M., Schirmer, R. H., and Karplus, P. A. (1998) *Nat. Struct. Biol. 5*, 267−271.
29. Demaster, E. G., Quast, B. J., Redfern, B., and Nagasawa, H. T. (1995) *Biochemistry 34*, 11494−11499.
30. Kim, K., Fettinger, J., Sessler, J. L., Cyr, M., Hugdahl, J., Collman, J. P., and Ibers, J. A. (1989) *J. Am. Chem. Soc. 111*, 403−405.
31. Kavanaugh, J. S., Weydert, J. A., Rogers, P. H., and Arnone, A. (1998) *Biochemistry 37*, 4358−4373.

BI9816711